# A Self-Tuning Passive Vibration Neutraliser using Nonlinear Coupling Between the Degrees-of-Freedom

Authors:

Gabriella Furlan Nehemy - gabriella.nehemy@unesp.br

State University of São Paulo - UNESP, School of Engineering, Bauru, Brazil

Emiliano Rustighi – emiliano.rustighi@unitn.it

University of Trento, Department of Industrial Engineering, Trento, Italy

Paulo J. Paupitz Gonçalves – paulo.paupitz@unesp.br

State University of São Paulo - UNESP, School of Engineering, Bauru, Brazil

Michael J. Brennan - mjbrennan0@btinternet.com

State University of São Paulo - UNESP, School of Engineering, Ilha Solteira, Brazil

**Abstract**

Vibration neutralisers are widely used to suppress vibration of a host structure subject to external excitation at a specific frequency. When attached to a structure, they create a notch filter in frequency response, reducing the vibration levels considerably. An inherent limitation is related to the narrow frequency range in which they are effective. Over the years, there have been different attempts to make the vibration absorber more robust. These attempts include using active and semi-active control strategies to change the tuning frequency, using piezoelectric elements with shunt circuits, electromagnetic actuators, servo motors, and even exploring nonlinear effects. In many cases, there is a need for an external power source to modify the characteristics of the system. In this paper, a vibration neutraliser that can adapt automatically to one of two frequencies corresponding to the frequency of an external harmonic force is described. Importantly it does this without the need for an external power source. The device consists of a beam-like neutraliser that is attached to the host structure at its centre through a roller bearing. The stiffness element is a rectangular beam that can rotate in the bearing, changing the stiffness it presents to the direction of excitation. The paper describes an experimental study into such a device, and an analytical model is proposed that qualitatively captures the time-domain behaviour of the experimental device. A possible mechanism by which the device self-tunes to either of the two frequencies of excitation is discussed. Supplementary material is also provided showing the device in operation.

# 1 Introduction

The vibration neutraliser consists of mass and stiffness elements tuned to a particular frequency, almost always related to an external harmonic force. This characteristic makes it different from the tuned vibration absorber that is often tuned to a resonance frequency of the host structure. Although they consist of similar elements, they have very different objectives. The neutraliser is commonly designed with relatively low damping to act as a mechanical notch-filter at a desired non-resonant frequency. Usually, the vibration absorber has an optimum damping value that could be relatively high to suppress vibration in a frequency range around a targeted resonance frequency.

In many practical engineering applications, the frequency of a vibration source is not constant, such as rotating machinery, propellers and reciprocating machines. In these conditions, the performance of the neutraliser can be compromised. A solution would require the neutraliser to adjust to the excitation frequency using an adaptation mechanism. This topic has been extensively studied, and there are some review articles describing this work [1–3].

Research on self-adaptive or self-tuning devices can be found in the literature. However, most of these absorbers and neutralisers require an external source to provide the adaptation capability. For instance, Buhr et al. [4], design a vibration absorber used in a four degree of freedom building model, where the absorber has a variable stiffness element which is adjusted using a motor and gearing mechanism. The stiffness is changed by rotating the spring through a collar and modifying the number of active spring coils. MacDaid and Mace [5] designed an electromechanical tuned vibration absorber with an adaptive synthetic shunt impedance. The adaptation requires the use of both feedforward and feedback control schemes to change the parameters of the shunt circuit to achieve the desired tuned frequency. A similar strategy was implemented by Hollkamp and Starchville [6] using piezoelectric transducers and shunt circuits.

An alternative design of a self-adaptive passive device is based on a mass on a string. This was explored by Acar and Yilmaz [7], who used a negative stiffness tension adjusting mechanism to change the natural frequency. Again, this required an external energy source to adjust the stiffness, using a motor and an external controller. Ghorbani-Tanha et al. [8] described a semiactive variable stiffness device in which the elastic

element consists of a rotational beam with a rectangular cross-section. The stiffness is controlled by an electrical motor that rotates the beam about its normal axis, causing a change in the second moment of area and consequently the stiffness in the desired direction. Again, this system required an external power source.

Rustighi [9] used a rotating stiffness element in a variable stiffness tunable absorber. The rotating stiffness element comprises of two springs with different stiffnesses arranged perpendicularly to each other and attached to a rotational mass. The rotation angle changes the effective absorber stiffness. Two configurations were experimentally investigated, and the broadest tuning range was obtained when two motors were used to rotate the two spring elements attached to the same mass. Also, using a rotating absorber stiffness element, Minaei and Ghorbani-Tanha [10] proposed a variable stiffness device using ball bearing and springs. An electric motor controlled the orientation of the springs to provide the required absorber stiffness. Alternative control strategies for tunable vibration absorbers have been discussed in [11–14].

The specific interest in this paper is the design of a passive self-tuning vibration neutraliser that does not require an external power source. However, only a few of such devices have been proposed in the literature. Sachau and Hanselka [15] designed a self-tuning absorber to track the rotational speed of a car engine. The device consisted of swing arms clamped to a disc in the radial direction. Each swing arm has a mass at its end. Because of the centrifugal force, which increases the geometric stiffness of the swing arms, the vibration absorber resonance frequency continuously adapts to the engine rotational speed. Another passive device was proposed by Ivers et al. [16]. The self-tuning vibration absorber consists of a cantilever beam with asymmetric damping at one end. The beam is threaded with a loosely threaded mass on it. The asymmetric damping induces the beam to whirl, and then the loose mass moves in a position that starts to resonate in opposition to the structural mass. The neutraliser considered in this work is based on the design proposed in a patent by Gustavsson [17], who also described some characteristics of the device in a conference paper [18]. It consists of a beam-like vibration neutraliser, where the beam has a rectangular cross-section, such that there are two different stiffnesses in orthogonal directions. The beam is placed inside a bearing allowing it to rotate around such that the stiffness in the direction of excitation changes as the rotation of the beam changes. The aim of the device is to self-tune to one of its two different natural frequencies to suppress vibration of a host structure at these frequencies.

Some numerical and experimental results were presented in [18], but an explanation into the physics governing the self-tuning mechanism was not provided.

The aim of this paper is to fill this gap. A device similar to that described by Gustavsson was built and tested, and an analytical model is proposed that contains a possible nonlinear mechanism by which the neutraliser self-tunes to either of two frequencies. The paper is organised into six sections, including this introductory text. A description of the neutraliser is given in Section two. In section three, the steady-state behaviour of the device is investigated both experimentally and analytically. A time-domain model is developed in section four to facilitate the understanding of how the device operates, which is discussed in relation to the experimental device in section five. Finally, the paper is closed with some conclusions in section six.

Five videos are provided as supplementary material. One is an animation showing the behaviour of the system point and transfer accelerance as a function of the angular configuration of the neutraliser. The other four videos show various aspects of the experimental device in operation.

## 2 Description of the device

The vibration neutraliser considered in this work is illustrated in Figure 1. It consists of a beam-like neutraliser that is attached to the host structure at its centre through a roller bearing and is designed to operate in the Y direction in the global coordinate reference system XYZ. The stiffness element is a rectangular beam that can rotate in the bearing about the Z-axis, as shown in the figure. Tip masses are attached at the ends of the beam. As the beam has a rectangular cross-section, two different orthogonal stiffnesses are defined in local coordinates that can rotate with respect to XYZ. Figure 1(a) depicts a side view of the device, and Figure 1(b) shows the beam set at three different angles, 0º, 45º and 90º.

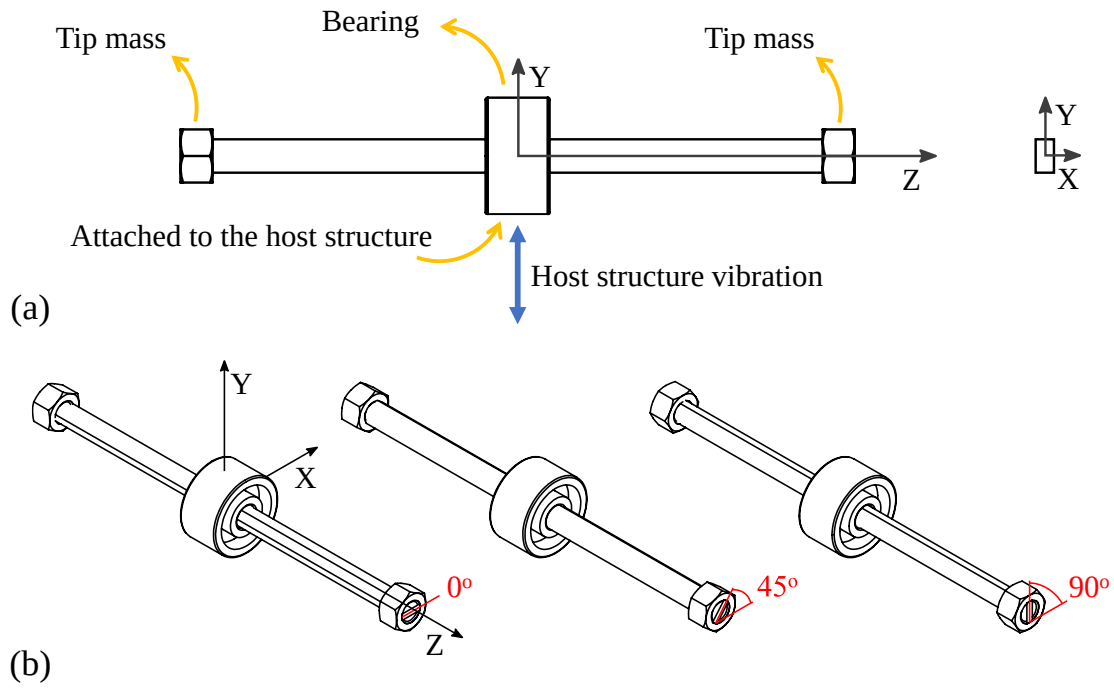


Figure 1. Schematic views of the device. (a) side view, (b) device configured at three different angles.

## 3 Steady-state behaviour with the beam set at fixed angles

Before carrying out time-domain experiments on the vibration neutraliser, the device was fixed at three angles $\theta = 0^{\circ}$, $\theta = 90^{\circ}$ and $\theta = 45^{\circ}$ as shown in Figure 1(b) and the steady-state responses were measured. The position $\theta = 0^{\circ}$ corresponds to when the cross-section of the beam is orientated so that the thinner part is horizontal and when $\theta = 90^{\circ}$ the thinner part is orientated so that it is vertical.

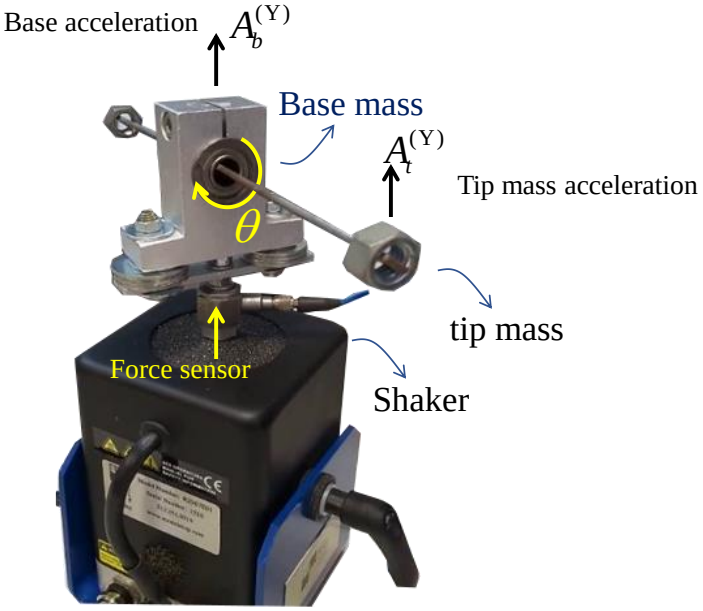


Figure 2. An illustration of the experimental test setup showing the shaker, force sensor at the base of the neutraliser.

The test setup is shown in Figure 2. The neutraliser was fixed to a Modal Shop type 2007E electromagnetic shaker through a PCB-208C01 force sensor. White noise was used to excite the system and the base and tip mass accelerations were measured using PCB-352C33, and PCB-352A59 accelerometers, respectively (not shown in the figure). All signals were recorded using an NI-USB 4431 board with a sampling frequency of 5 kHz. Point and transfer accelerances (acceleration/force) were estimated using the $H_1$ transfer function estimator in LabView. Hanning windows of 10 second duration were used in the transformation of the data from the time to the frequency domain, and 30 averages were taken.

The experimental results are shown in Fig. 3. The point accelerance, is shown in the left-hand set of graphs and is given by $|A_b^{(Y)}/F|$, where $A_b^{(Y)}$ is the spectrum of the acceleration of the base mass in the Y direction and $F$ is the spectrum of the applied force. The transfer accelerance, is shown in the right-hand set of graphs and is given by $|A_t^{(Y)}/F|$, where $A_t^{(Y)}$ is the spectrum of the acceleration of the tip mass in the Y direction. Also shown in this figure are thin solid lines which are obtained from a simplified model of the device, which is discussed next.

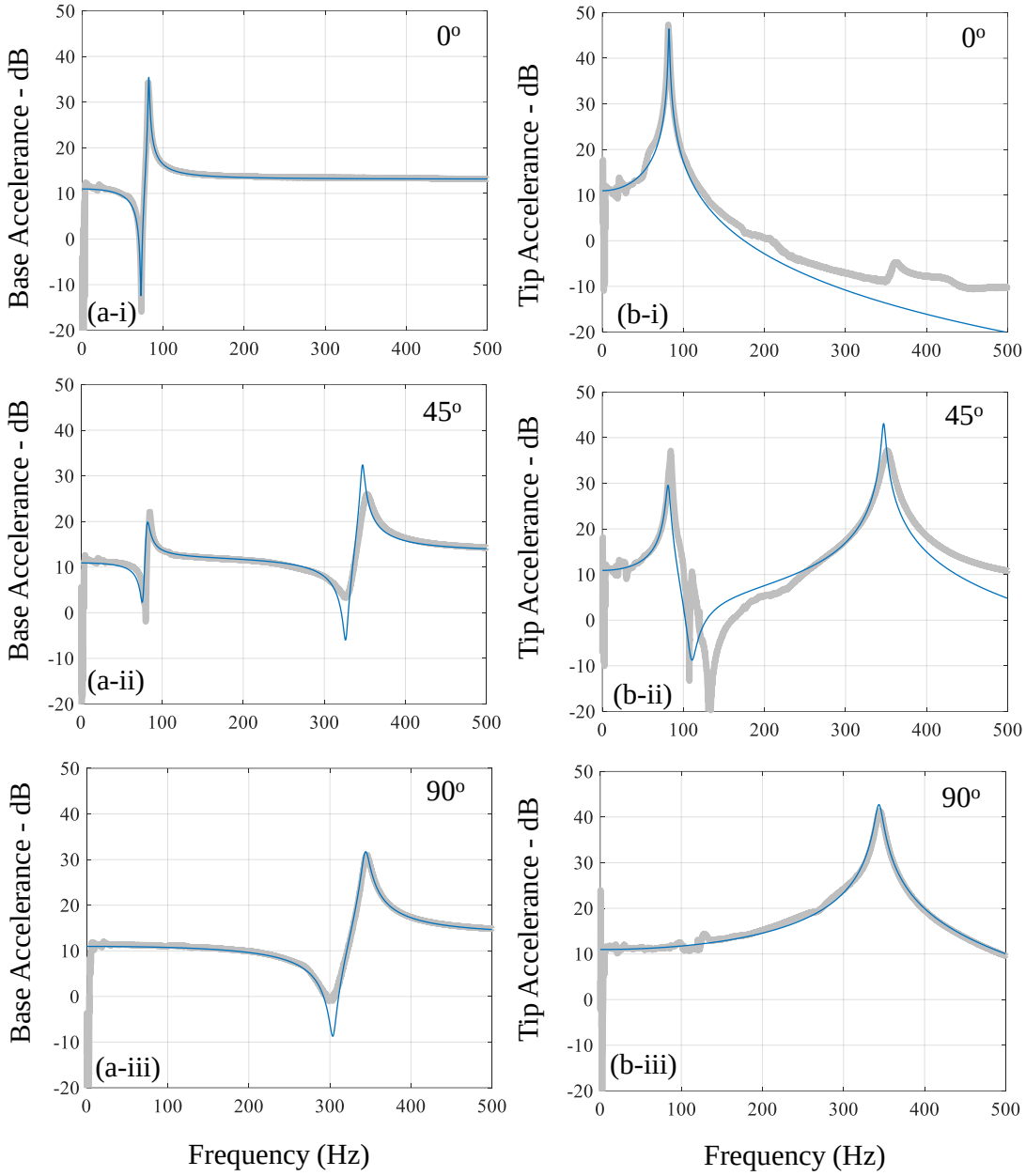


Figure 3. The magnitudes of the accelerances for different angles. The thin blue lines are the model responses, and the thick grey lines are the experimental responses. Subfigures (a) are the base accelerance $|A_b^{(Y)}/F|$ and subfigures (b) are the tip accelerance $|A_t^{(Y)}/F|$. (dB ref. 1 Ns$^2$/m).

To gain some physical insight into the steady-state behaviour of the neutraliser, when the beam is set at different angles, a model of the device is developed. The model is also used to estimate some key parameters of the neutraliser which are used in time domain simulations described in section 4. A photograph of the neutraliser is shown in Figure 4(a), and a simple model of the device is depicted in Figure 4(b). The device is symmetric about the point of excitation, and the stiffnesses of the beam on either side of the central

bearing are denoted by $k_{xx}$ and $k_{yy}$, which are defined in local coordinates xy. Each tip mass is denoted by $m_t$ and the polar moment of inertia $J$ around the Z-axis comprises the beam, the tip mass moments and bearing inner ring altogether. The bearing support block, outer bearing ring and fixing part masses are all lumped together to give the base mass $m_b$.

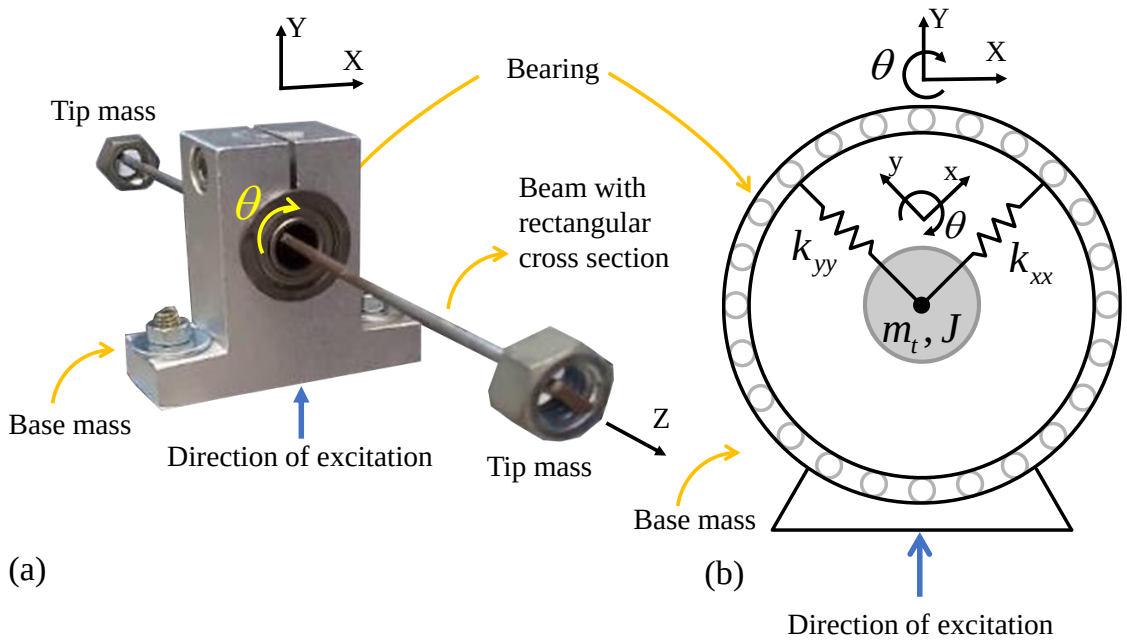


Figure 4. (a) A photograph of the neutraliser and a (b) schematic of the lumped parameter model showing the local (xyz) and global (XYZ) coordinate systems.

A simplified lumped parameter frequency domain model of the neutraliser can be written down as

$$\mathbf{T}^{\mathrm{T}}\left(-\omega^2\mathbf{M}+i\omega\mathbf{C}+\mathbf{K}\right)\mathbf{T}\mathbf{q}=\mathbf{f}\,, \tag{1}$$

where **M**, **K** and **C** are the mass, stiffness and viscous damping matrices, respectively given by

$$\mathbf{M}=\begin{bmatrix} m_b & 0 & 0 & 0 \\ 0 & m_b & 0 & 0 \\ 0 & 0 & m_t & 0 \\ 0 & 0 & 0 & m_t \end{bmatrix}, \mathbf{K}=\begin{bmatrix} k_{xx} & 0 & -k_{xx} & 0 \\ 0 & k_{yy} & 0 & -k_{yy} \\ -k_{xx} & 0 & k_{xx} & 0 \\ 0 & -k_{yy} & 0 & k_{yy} \end{bmatrix}, \quad \text{(2a,b,c)}$$

$$\mathbf{C}=\begin{bmatrix} c_{xx} & 0 & -c_{xx} & 0 \\ 0 & c_{yy} & 0 & -c_{yy} \\ -c_{xx} & 0 & c_{xx} & 0 \\ 0 & -c_{yy} & 0 & c_{yy} \end{bmatrix}$$

in which $c_{xx}$ and $c_{yy}$ $c_\theta$ viscous damping coefficients, artificially added to take into account the damping mechanisms in the device; **T** is a coordinate transformation matrix given by

$$\mathbf{T}=\begin{bmatrix} \cos(\theta) & \sin(\theta) & 0 & 0 \\ -\sin(\theta) & \cos(\theta) & 0 & 0 \\ 0 & 0 & \cos(\theta) & \sin(\theta) \\ 0 & 0 & -\sin(\theta) & \cos(\theta) \end{bmatrix} \quad \text{(2d)}$$

where corresponds to the angle shown in Fig. 3, at which the beam is rotated with respect to the origin; $\mathbf{q}=\begin{bmatrix} Q_b^{(\mathrm{X})} & Q_b^{(\mathrm{Y})} & Q_t^{(\mathrm{X})} & Q_b^{(\mathrm{Y})} \end{bmatrix}^{\mathrm{T}}$ $\mathbf{q}=\begin{bmatrix} Q_b^{(\mathrm{X})} & Q_b^{(\mathrm{Y})} & Q_t^{(\mathrm{X})} & Q_b^{(\mathrm{Y})} & \Theta \end{bmatrix}^{\mathrm{T}}$ is the displacement vector, where $Q_b$ and $Q_t$ ($\Theta$) are complex amplitudes of the base and tip in the X and Y directions; $\mathbf{f}=\begin{bmatrix} 0 & F & 0 & 0 \end{bmatrix}^T$ $\mathbf{f}=\begin{bmatrix} 0 & F & 0 & 0 & 0 \end{bmatrix}^T$ is the force vector in which $F$ is the amplitude of the force applied in the Y direction; $(\,)^{\mathrm{T}}$ denotes the matrix or vector transpose. The moment of inertia $J$ does not appear in equations 2(a) because the analysis in this section is done using fixed angles.

The parameters of the model were estimated qualitatively by setting the low and high frequencies asymptotes and matching the resonance frequencies. Later, the viscous damping was adjusted manually such that the peaks of the model and experiments have similar magnitudes. The identified parameters of the model are shown in Table 1.

Table 1. Parameters estimated from the experimental tests

| **Property** | **Value** |
|---|---|
| Base mass $(m_b)$ | 0.2210 kg |
| Tip mass $(m_t)$ | 0.0638 kg |
| Stiffness in x direction $(k_{xx})$ | 12900.0 N/m |
| Stiffness in y direction $(k_{yy})$ | 235300.0 N/m |
| Viscous damping in x direction $(c_{xx})$ | 2.7 Ns/m |
| Viscous damping in y direction $(c_{yy})$ | 0.42 Ns/m |

The point and accelerances calculated using the model were obtained by multiplying the complex displacements by the square of the circular frequency, i.e., $\left|A_b^{(\mathrm{Y})}\right| = \left|\omega^2 Q_b^{(\mathrm{Y})}\right|$ and $\left|A_t^{(\mathrm{Y})}\right| = \left|\omega^2 Q_t^{(\mathrm{Y})}\right|$. The resulting accelerances using the estimated parameters from Tab. 1 are shown as thin solid lines in Fig. 2. The magnitudes of the accelerances shown in Figure 2 (i, ii and iii) correspond to the fixed angles $\theta = 0^\circ$, $90^\circ$ and $45^\circ$, respectively. Figures 2(a) and 2(b) show the comparison of the model and experimental accelerances measured at the base and at the tip mass, respectively.

The model and experimental results generally show good agreement, except at some frequencies, such as at approximately 100 Hz, which can be seen in Figure 4(a-iii). This is probably because of a torsional resonance that has not been modelled.

It is also important to note a small difference between the experiment antiresonance frequencies and the model, which must be considered in the discussion presented in section four.

The following observations can be made:

1. The natural frequencies of the system do not change with the angular position of the device.
2. In general, the frequency responses are sensitive to the angle, mainly at the antiresonance frequencies. To explore this further, the way in which the antiresonance frequencies change as a function of $\theta$ are plotted in Fig. 5 using the model. Figure 5(a) shows the model base accelerance and Figure 5(b) shows the model tip accelerance when $\theta = 45^{\circ}$. There are two resonance frequencies $f_1$ and $f_2$ which are fixed. The frequency $f_3$ is the antiresonance for the tip response. Frequencies $f_4$ and $f_5$ are antiresonance frequencies for the base response.
3. The antiresonance frequencies $f_4$ and $f_5$ are equivalent to the natural frequencies of a cantilever beam (base mass is fixed) with a tip mass. Here they correspond to $f_4 = \sqrt{k_{xx} / m_t}$ and $f_5 = \sqrt{k_{yy} / m_t}$ (only when $\theta$ = 0º and 90º, respectively, when the two equations are uncoupled). These frequencies are used in the model discussed in section 4.
4. Figure 5(c) shows how these frequencies change according to the value of the angle $\theta$. It is notable that the antiresonance frequency $f_3$, varies from the second resonance when $\theta = 0^{\circ}$ to the first resonance when $\theta = 90^{\circ}$.
5. When $\theta = 0^{\circ}$, resonance frequency $f_2$, and antiresonance frequencies $f_3$ and $f_5$ merge, counteracting the second resonance. This results in a single resonance frequency $f_1$.
6. When $\theta = 90^{\circ}$ the resonance frequency $f_1$ merges with antiresonance frequencies $f_3$ and $f_4$, counteracting the first resonance. This results in a single resonance frequency $f_2$. These effects can be observed in the [**supplementary material – video 1**]

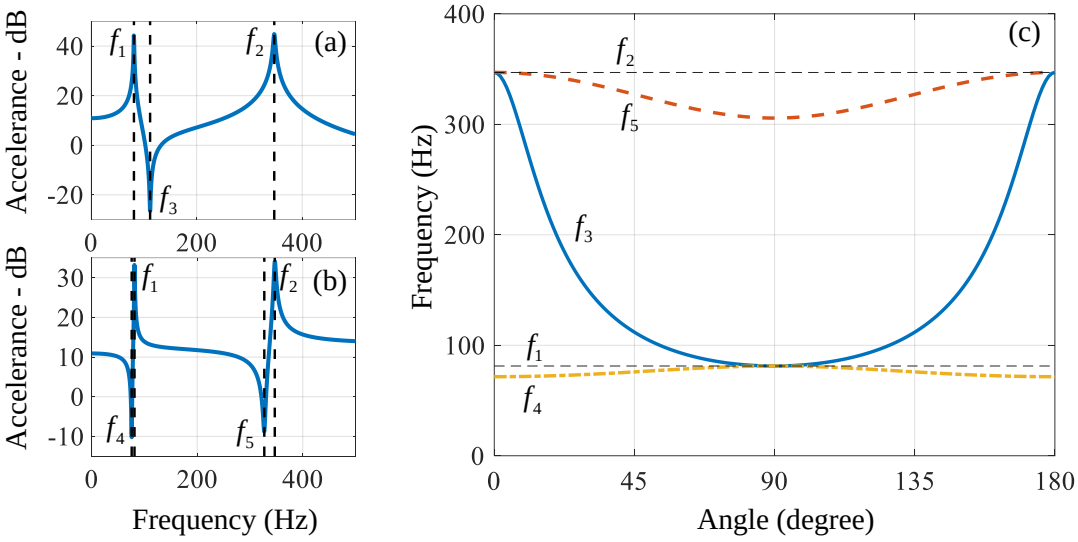


Figure 5. Resonance and antiresonance behaviour as a function of $\theta$. (a) tip accelerance for $\theta = 45^{\circ}$, (b) base accelerance for $\theta = 45^{\circ}$ (dB ref. 1 N.s$^2$/m), (c) Behaviour of the resonance and antiresonance as $\theta$ varies between 0 and 180$^o$.

## 4 Harmonic excitation with the beam free to rotate

The intended use for the vibration neutraliser is that it can track an excitation force to self-tune to either of the two antiresonance frequencies at 73 Hz or 295 Hz, these are the measured antiresonance at 0$^o$ and 90$^o$, respectively, such that vibration of a host structure is reduced at these frequencies. This behaviour is demonstrated experimentally, and a simplified model is proposed to explain why the device rotates and self-tunes to the excitation frequency.

Experimental tests were performed with the neutraliser free to rotate. The set-up was similar to that in Fig. 2, but the vertical displacement of the tip mass and the angular displacement of the beam were measured using a SONY Camera RX100-V at 960 frames per second to avoid the accelerometer cable interfering with the beam rotation. The base acceleration was measured using a PCB-352C33 accelerometer, and was recorded using the NI-USB 4431 data acquisition system with a sampling frequency of 5 kHz. The vertical displacement of the tip mass and the angular displacement of the beam were extracted from the recorded movie using Tracker software [19]. To enable the base motion to be compared with the tip vibration, the measured acceleration time history is integrated numerically to give the base displacement as a function of time. The time histories obtained from the camera and the accelerometer were synchronised using correlation.

Two experiments were conducted. First, the neutraliser was arranged with the angle $\theta = 0^{\circ}$. The system was then excited at a fixed frequency of 295 Hz, see the [**supplementary material - video 2**]. The results of this test are shown in Figure 6.

Figure 6(a) shows the tip angular displacement changing from $\theta = 0^{\circ}$ to approximately $\theta = 100^{\circ}$. The tip mass displacement increases (Figure 9(a-ii)), while the base displacement is reduced (Figure 9(a-iii)). This illustrates the effectiveness of the neutraliser to reduce vibration on a host structure, here represented as the base displacement.

The second procedure initially arranged the neutraliser with angle $\theta = 90^{\circ}$ and excited at fixed frequency sine force at 73 Hz, see the [**supplementary material – video 3**].

The results of this test are shown in Figure 9b. Figure 9(b-i) shows the angular displacement of the tip mass changing from $\theta = 90^{\circ}$ to approximately $\theta = 7^{\circ}$. The tip displacement is shown in Figure 9(b-ii) and base displacement in Figure 9(b-iii).

It should be pointed out that the device requires some amplitude to rotate. In general, the base acceleration needs to be higher than 1 g to allow the device to adapt. Also, friction damping for the rotation greatly influences how fast the device tunes itself. Higher friction requires higher excitation levels to allow the device to self-adjust to the excitation frequency. Some other supplementary videos show the neutraliser in operation [**supplementary materials - video 4, video 5**].

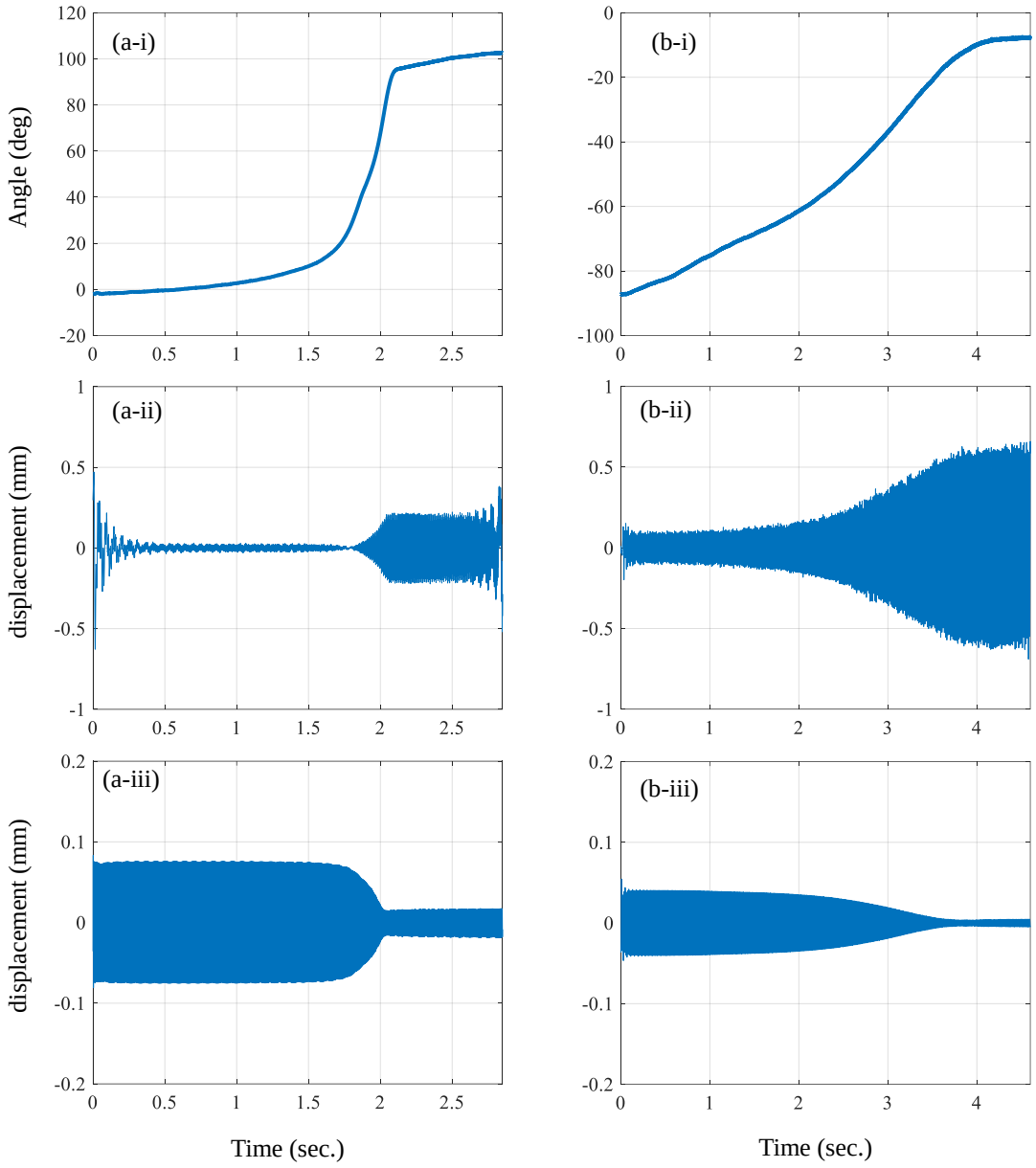


Figure 6. Time histories for fixed harmonic excitation. (a) excited at 295 Hz and (b) excited at 73 Hz. Subfigures (i) are the angular displacement, subfigures (ii) are the tip displacement and subfigures (iii) are the base displacements for the two experimental procedures.

The physical behaviour of the self-tuning neutraliser can be reproduced by a lumped-parameter, three degrees-of-freedom model, considering the tip displacements in the XY axis, plus the rotation around the Z-axis, represented by $\theta$. The mechanical model is that shown in Fig. 2(b) with the beam able to rotate, and with harmonic excitation of the base. A time domain model is now required, however, so the variables $q_x$ and $q_y$ are introduced to describe the translational motion of the mass suspended at the end of the cantilever

beam in the X and Y directions. As before, the variable $\theta$ describes the rotation of the mass-spring assembly. In this case, the central support (base of the neutraliser) is assumed to be massless since its displacement has been imposed vertically and constrained horizontally. A harmonic base excitation, $q_b^{(Y)} = A\cos(\omega t)$, is assumed as the external forcing excitation.

The equation of motion of the system is obtained using Lagrange's method. The kinetic energy of the system is given by

$$T = \frac{1}{2}m\left(\dot{x}^2 + \dot{y}^2\right) + \frac{1}{2}I\dot{\theta}^2 \tag{3}$$

The potential energy is due to the gravitational field and the strain energy stored in the springs. The deformation of the two-springs depends on $\theta$ and the relative motion between the base and the suspended mass, so that

$$V = mgq_y + \frac{1}{2}\begin{Bmatrix} q_x \\ y - A\cos(\omega t) \end{Bmatrix}^{\mathrm{T}} \begin{bmatrix} k_{11}(\theta) & k_{12}(\theta) \\ k_{21}(\theta) & k_{21}(\theta) \end{bmatrix} \begin{Bmatrix} q_x \\ y - A\cos(\omega t) \end{Bmatrix} \tag{4}$$

where $\begin{bmatrix} k_{11}(\theta) & k_{12}(\theta) \\ k_{21}(\theta) & k_{21}(\theta) \end{bmatrix} = \begin{bmatrix} (k_{xx} - k_{yy})\cos(\theta)^2 + k_{yy} & (k_{xx} - k_{yy})\cos(\theta)\sin(\theta) \\ (k_{xx} - k_{yy})\cos(\theta)\sin(\theta) & (k_{yy} - k_{xx})\cos(\theta)^2 + k_{xx} \end{bmatrix}$

Three equations of motion are obtained as follows,

$$\begin{aligned} &I\dot{\theta} + c_\theta\dot{\theta} + \frac{1}{2}(k_{xx} - k_{yy})[-\sin(2\theta)q_x^2 + 2\cos(2\theta)q_x q_y + \sin(2\theta)q_y^2] = \\ &\frac{1}{4}(k_{xx} - k_{yy})\{-\sin(2\theta)A^2 + 4A[\cos(2\theta)q_x + \sin(2\theta)q_y]\cos(\omega t) - \\ &A^2\sin(2\theta)\cos(2\omega t)\} \end{aligned} \tag{5a}$$

$$\begin{aligned} &m_t\ddot{q}_x + c_x\dot{q}_x + [k_{xx}\cos^2(\theta) + k_{yy}\sin^2(\theta)]q_x + (k_{xx} - k_{yy})\cos(\theta)\sin(\theta)q_y = \\ &(k_{xx} - k_{yy})\cos(\theta)\sin(\theta)A\cos(\omega t) \end{aligned} \tag{5b}$$

$$m_t\ddot{q}_y + c_y\dot{q}_y + [k_{xx}\sin^2(\theta) + k_{yy}\cos^2(\theta)]q_y + (k_{xx} - k_{yy})\cos(\theta)\sin(\theta)q_x = [k_{xx}\sin^2(\theta) + k_{yy}\cos^2(\theta)]A\cos(\omega t) = 0 \quad (5c)$$

to which some viscous damping term has been added to include a dissipation mechanism. Equations (5b) and (5c) represents the equation of a point mass on a plane constrained by an orthotropic spring. They are coupled by the out-of-plane terms in the stiffness matrix. The elastic forces depend on the angular orientation of the device and in this sense they are characteristic of an auto-parametric system [20,21]. Equations (5b) and (5c) are not inherently nonlinear. However, if the system is rotating, the stiffness is time-variant and this could potentially give rise to parametric excitation. Equation (8a) is nonlinear due to the trigonometric terms in the equation. When the mass is displaced, the elastic forces applied to the inner ring of the bearing result in a none-zero elastic torque as illustrated in Figure 7. Since the torque is obtained by multiplying the elastic forces (proportional to displacements) by their arm, the elastic torque depends on quadratic terms of the displacement.

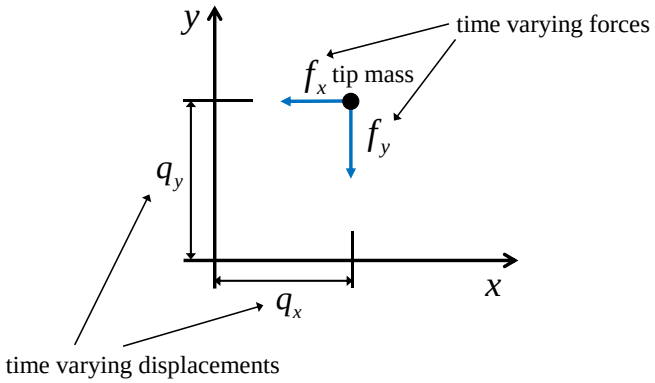


Figure 7. Elastic forces due to the mass displacement resulting in a torque.

$$f_x = [k_{xx}\cos^2(\theta) + k_{yy}\sin^2(\theta)]q_x + (k_{xx} - k_{yy})\cos(\theta)\sin(\theta)q_y \text{ and}$$

$$f_y = [k_{xx}\sin^2(\theta) + k_{yy}\cos^2(\theta)]q_y + (k_{xx} - k_{yy})\cos(\theta)\sin(\theta)q_x$$

The same observation can be applied to the forced vibration equations. The sinusoidal base excitation translates into a quadratic torque term. The quadratic term occurs because the torque is the product of the elastic forces and a mass displacement term which are both sinusoidal, i.e., harmonic at the frequency of excitation. Hence, the excitation term has a sinusoidal component at frequency $\omega$ a sinusoidal component at $2\omega$ and a constant

step-like term $\left(\frac{k_{yy}-k_{xx}}{2}\right)\sin(\theta)\cos(\theta)A^2$. The latter term becomes zero when $\theta = 0°$ or $90°$. The harmonic excitation term at frequency $\omega$ is found to be negligible as it depends on $A$ instead of $A^2$. The harmonic excitation term at frequency $2\omega$ also seems to generate negligible components compared to the large rotation due to the constant term. Given that the rotation mainly responds to this term and it changes relatively slowly, no parametric excitation phenomena is observed.

The nonlinear system of the equations of motion is integrated numerically to simulate the physical response to see if it is similar to the experimental results. Figure 8 shows the numerical results. The system is excited with a sinusoidal base excitation at either 71 or 300 Hz, which are approximately the two resonance frequencies of model. These resonance frequencies are associated with the antiresonance of the experimental system when the vibration neutraliser is attached to a host structure as seen in the previous section.

The results are compared with the case in which the system is free to rotate and the case in which the rotation is constrained. The system rotates so that the resonance frequency of the system coincides with that of the system aligned to direction of the excitation. Hence, the system is able to self-tune to each of the two resonance frequencies. The system rotation is driven by a second-order system, and exhibits no overshoot since the rotational behaviour of the system is overdamped (representing the same behaviour as the experimental rig). Once the system is in the tuned position, the constant term of excitation becomes negligible, and no further rotation is recorded.

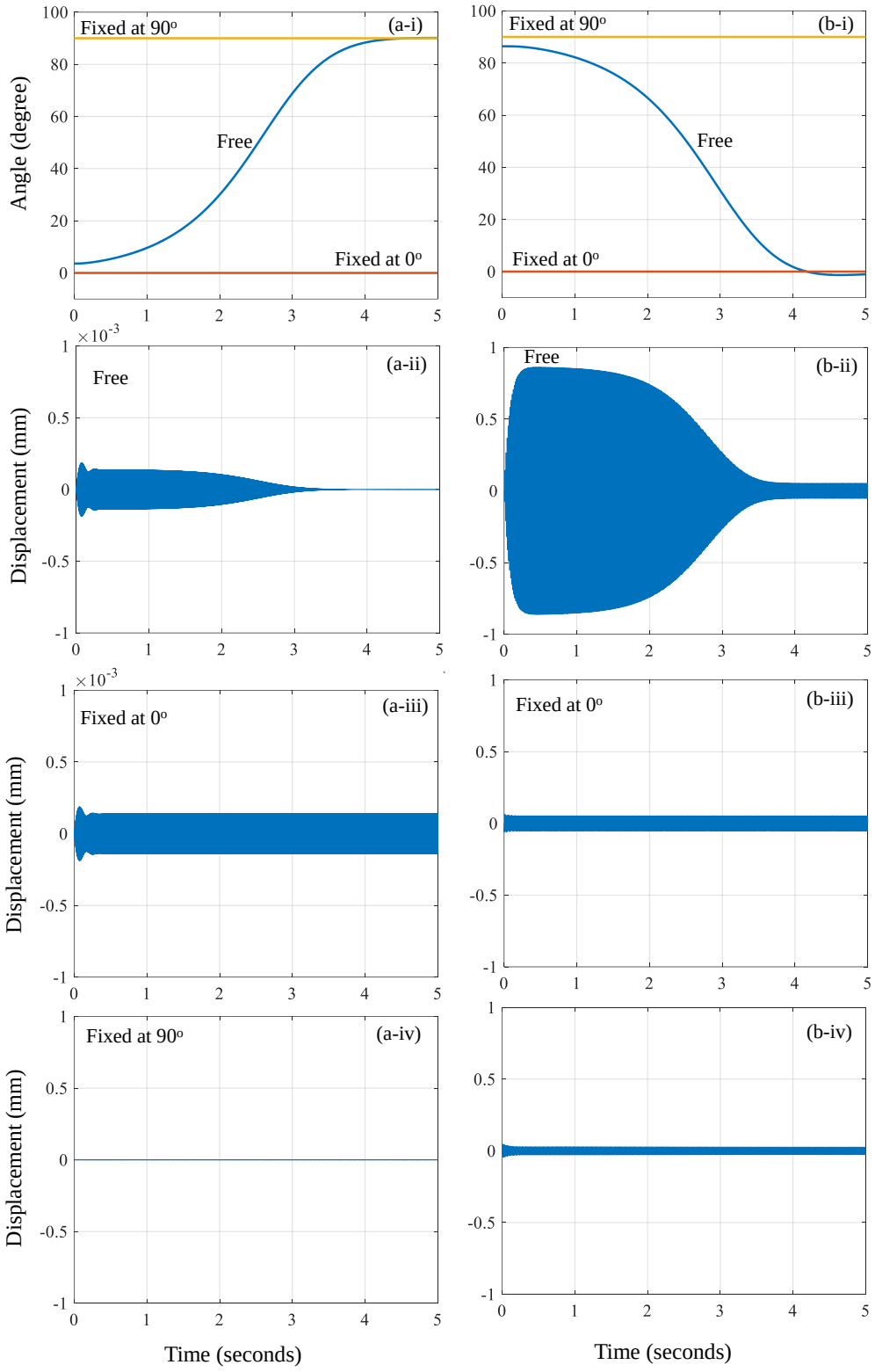


Figure 8. Numerical simulation for sinusoidal excitation at the lower (a) and higher (b) resonance frequency: (a) 71 Hz excitation with base acceleration of 10 $ms^{-2}$; (b) 300 Hz excitation with base acceleration of 20 $ms^{-2}$; (i) rotation for the system free to rotate or blocked at 0 or 90 degrees; vertical mass displacement for free rotation (ii), for system blocked at 0 degrees (iii) and for system blocked at 90 degrees (iv).

# 5 Discussion

The experimental results and model output show a strong qualitative agreement. They both show the ability of the device to self-tune or spin the beam so that the structure is excited at a resonance frequency. Such behaviour has demonstrated that the device can self-tune to two resonance frequencies. The time responses of the experimental device and the model have some differences, resulting in some dissimilarities which have been minimised by the manual optimisation of two parameters, namely the torsional damping coefficient and the amplitude of the base oscillations. These were chosen to obtain a similar time response of the rotation of the neutraliser in terms of the rise time and overshoot. In the model, the beam rotates with the same rise time but with smaller base acceleration than in the experimental device, which is possible because there is some play and friction in the bearing, which were not accounted for in the model. The effect of such a simplification may also be seen in the effects caused by the choice of the initial conditions. In the model, it is necessary to use an initial condition which is slightly different to zero or ninety degrees for the beam to rotate from one position to another. This was not necessary in the experimental device because of inevitable mechanical imperfections, which meant that the bearing system was not strictly symmetrical, making small initial rotations possible. When a small rotation is present, the moment due to the deformation of the beam causes the self-tuning of the device.

The most significant difference between the model and the experiment is, however, in the way the systems are excited. In the experimental device the excitation is in the form of a force applied by the shaker table. In the model, a base motion excitation was applied, which was done to minimise the number of degrees-of-freedom, but at the same time being able to describe the physical behaviour of the system. Also, such a model is similar to that of a spring pendulum, which is a model that exhibits auto-parametric excitation. Although the accelerance function of the base cannot be obtained from this model, the tip accelerations show similar behaviour to those measured in the experimental results. Note that at the two extreme angular positions of 0° and 90°, which correspond to the tuned frequencies of the device, the natural frequency of the beam tip in the time domain model corresponds to an antiresonance of the base mass in the steady-state model. Such correspondence is not exact for the other angular positions due to the cross term in the stiffness matrix. However, the shift in the antiresonance with the angular position may increase the robustness of the actual device due to the fact that the antiresonance tuning

range is slightly increased, as seen in Figure 5(c). Despite the difference between the experimental device and the model, and the limitations of the model, it can be seen that it captures the general behaviour of the experimental neutraliser and provides a possible mechanism by which the device self-tunes.

## 6 Conclusions

This paper has described a vibration neutraliser that can passively self-tune to either of two natural frequencies in response to an external excitation source. The device is a beam-like neutraliser, in which a rectangular beam can rotate freely within a roller bearing at the centre of the beam, which is fixed to a host structure. The two tuned frequencies correspond to when the beam is aligned such that the thinner beam cross-section or the thicker beam cross-section align with the direction of excitation. The device has been studied experimentally with steady-state excitation for fixed rotational angles of the beam, and with harmonic excitation when the beam is allowed to rotate to its optimum position. The system has also been modelled when the beam angle is fixed to gain physical insight into the system behaviour and to obtain physical parameters that were used in the time domain model, which was used to investigate the self-tuning behaviour. The model illustrates a likely mechanism for the self-tuning properties. This is a time varying moment that is the product of a time varying force due to the vibrating tip mass, and a time varying moment arm. The result is a dominant DC moment whose magnitude is a function of the difference between the excitation frequency and the target natural frequency of the device, which diminishes as the natural frequency approaches the excitation frequency. The work discussed here opens the possibility of improving the robustness of neutralisers that are only effective at a narrow frequency range.

## Acknowledgments

We gratefully acknowledge support of CNPq - National Council for Scientific and Technological Development (Grant Number 406594/2021-0), FAPESP – São Paulo Research Foundation (Grant Number 2018/15894-0) and CAPES - National Council for the Improvement of Higher Education (Grant Number 88887.513387/2020-00)

## References


[1] M.J. Brennan, Some recent developments in adaptive tuned vibration absorbers/neutralisers, Shock and Vibration. 13 (2006) 531–543. https://doi.org/10.1155/2006/563934.

[2] J.Q. Sun, M.R. Jolly, M.A. Norris, Passive, adaptive and active tuned vibration absorbers-a survey, Journal of Mechanical Design, Transactions of the ASME. 117 (1995) 234–242. https://doi.org/10.1115/1.2836462.

[3] R.R.A. Ibrahim, Recent advances in nonlinear passive vibration isolators, Journal of Sound and Vibration. 314 (2008) 371–452. https://doi.org/10.1016/j.jsv.2008.01.014.

[4] C.A. Buhr, M.A. Pranchek, R.J. Bernhard, Noncollocated adaptive-passive vibration control using self-tuning vibration absorbers, in: Proceedings of the American Control Conference, 1998: pp. 3460–3464. https://doi.org/10.1109/ACC.1998.703240.

[5] A.J. McDaid, B.R. Mace, A Robust Adaptive Tuned Vibration Absorber Using Semi-Passive Shunt Electronics, IEEE Transactions on Industrial Electronics. 63 (2016) 5069–5077. https://doi.org/10.1109/TIE.2016.2554541.

[6] J.J. Hollkamp, T.F. Starchville, A Self-Tuning Piezoelectric Vibration Absorber, Journal of Intelligent Material Systems and Structures. 5 (1994) 559–566. https://doi.org/10.1177/1045389X9400500412.

[7] M.A. Acar, C. Yilmaz, Design of an adaptive-passive dynamic vibration absorber composed of a string-mass system equipped with negative stiffness tension adjusting mechanism, Journal of Sound and Vibration. 332 (2013) 231–245. https://doi.org/10.1016/j.jsv.2012.09.007.

[8] A.K. Ghorbani-Tanha, M. Rahimian, A. Noorzad, A Novel Semiactive Variable Stiffness Device and Its Application in a New Semiactive Tuned Vibration Absorber, Journal of Engineering Mechanics. 137 (2011) 390–399. https://doi.org/10.1061/(asce)em.1943-7889.0000235.

[9] E. Rustighi, A tuneable vibration absorber based on rotating stiffness elements, in: Proceedings of the Tenth International Conference on Recent Advances in Structural Dynamics (RASD2010), Southampton, 2010.

[10] A. Minaei, A.K. Ghorbani-Tanha, Optimal Step-by-Step Tuning Method for Variable Stiffness Semiactive Tuned Mass Dampers, Journal of Engineering Mechanics. 145 (2019) 04019037. https://doi.org/10.1061/(asce)em.1943-

7889.0001610.

[11] M.R.F. Kidner, M.J. Brennan, Varying the stiffness of a beam-like neutralizer under fuzzy logic control, Journal of Vibration and Acoustics, Transactions of the ASME. 124 (2002) 90–99. https://doi.org/10.1115/1.1423634.

[12] J.P. Carneal, F. Charette, C.R. Fuller, Minimization of sound radiation from plates using adaptive tuned vibration absorbers, Journal of Sound and Vibration. 270 (2004) 781–792. https://doi.org/10.1016/S0022-460X(03)00257-8.

[13] S.T. Wu, Y.J. Shao, Adaptive vibration control using a virtual-vibration-absorber controller, Journal of Sound and Vibration. 305 (2007) 891–903. https://doi.org/10.1016/j.jsv.2007.04.046.

[14] T. Long, M.J. Brennan, S.J. Elliott, Design of smart machinery installations to reduce transmitted vibrations by adaptive modification of internal forces, Proceedings of the Institution of Mechanical Engineers. Part I: Journal of Systems and Control Engineering. 212 (1998) 215–227. https://doi.org/10.1243/0959651981539415.

[15] D. Sachau, J. Hanselka, Multi-body-Simulation of a Self Adaptive Torsional Vibration Absorber, Conference Proceedings of the Society for Experimental Mechanics Series. 45 (2014) 85–91. https://doi.org/10.1007/978-1-4614-6585-0_8.

[16] D. Ivers, R. Wilson, D. Margolis, Whirling-beam self-tuning vibration absorber, Journal of Dynamic Systems, Measurement and Control, Transactions of the ASME. 130 (2008). https://doi.org/10.1115/1.2907399.

[17] M. Gustavsson, A device for reducing Vibrations and Sounds, U.S. Patent Application No. 11/883,094., 2011.

[18] M. Gustavsson, A self-adaptive resonant device and its use for noise control in turbo-prop aircraft, in: INTER-NOISE and NOISE-CON Congress and Conference Proceedings, 2016: pp. 1353–1359.

[19] D. Brown, R. Hanson, W. Christian, Tracker Video Analysis and Modeling Tool, (2022). https://physlets.org/tracker/.

[20] A.H. Nayfeh, D.T. Mook, Nonlinear Oscillations, John Wiley & Sons, 2008.

[21] J.J. Thomsen, Vibrations and stability, Springer-Verlag, 2003.